RSC Advances

PAPER

View Article Online
View Journal | View Issue

Cite this: *RSC Adv.*, 2021, **11**, 11519

Supramolecular gel formation regulated by water content in organic solvents: self-assembly mechanism and biomedical applications†

Lieqiang Liao, ‡[ab] Xinjian Jia, ‡[b] Haoxiang Lou, [b] Jinlian Zhong, [b] Huijin Liu, [b] Shunming Ding, [a] Chao Chen, *[a] Sanguo Hong*[a] and Xuzhong Luo *[b]

As one of the most important and fruitful methods, supramolecular self-assembly has a significant advantage in designing and fabricating functional soft materials with various nanostructures. In this research, a low-molecular-weight gelator, *N*,*N*′-di(pyridin-4-yl)-pyridine-3,5-dicarboxamide (PDA-N4), was synthesized and used to construct self-assembled gels *via* a solvent-mediated strategy. It was found that PDA-N4 could form supramolecular gels in mixed solvents of water and DMSO (or DMF) at high water fraction (greater than or equal to 50%). By decreasing the water fraction from 50% to 30%, the gel, suspension and solution phases appeared successively, indicating that self-assembled aggregates could be efficiently modulated *via* water content in organic solvents. Moreover, the as-prepared PDA-N4 supramolecular gels not only displayed solid-like behavior, and pH- and thermo-reversible characteristics, but also showed a solution–gel–crystal transition with the extension of aging time. Further analyses suggested that both the crystal and gel had similar assembled structures. The intermolecular hydrogen bonding between amide groups and the π–π stacking interactions between pyridine groups played key roles in gel formation. Additionally, the release behavior of vitamin B12 (VB_{12}) from PDA-N4 gel (H_2O/DMSO, v/v = 90/10) was evaluated, and the drug controlled release process was consistent with a first-order release mechanism. The human umbilical venous endothelial cell culture results showed that the PDA-N4 xerogel has good cytocompatibility, which implied that the gels have potential biological application in tissue engineering and controlled drug release.

Received 25th January 2021
Accepted 2nd March 2021

DOI: 10.1039/d1ra00647a

rsc.li/rsc-advances

1. Introduction

Inspired by the intriguing molecular self-assembly in nature, it is becoming increasingly attractive to mimic supramolecular self-assembled structures by small molecular components *via* various non-covalent interactions (*e.g.* hydrogen bonding, π–π stacking, metal coordination, van der Waals interactions, hydrophobic interactions, *etc.*).[1] Generally speaking, individual molecules could self-assemble into a series of nano/micro-aggregates including fibers, sheets, tubes, micelles, hollow spheres, helixes, vesicles, *etc.* when encountering special variations in self-assembly conditions, and exhibit fascinating chemical, physical and optical properties.[2] Nevertheless, the development and application of functional supramolecular self-assemblies, especially those which could be effectively controlled by changing the environment, will still be full of challenges.

In recent years, various exoteric conditions such as assembly rate, redox potentials, ultrasound, environmental pH and solvents have been investigated in tuning self-assembled structures.[3–7] Among these approaches, the solvent-mediated strategy is regarded as a most simple and effective method, in which solvent molecules could significantly involve in the self-assembly processes.[8] Moreover, a variety of parameters including polarity, viscosity, refractive index, solubility, boiling point and chirality are critical to the nucleation and growth process of self-assemblies.[9] Based on the nature of substitute, solvent polarity and concentration, Li's group designed controllable nanostructures (nanowires, nanospheres, nanosheets and nanobelts) with tunable dimensions *via* self-assembly of L-lysine-functionalized perylene bisimides. For each obtained supramolecular

[a]*Key Laboratory of Jiangxi Province for Environment and Energy Catalysis, College of Chemistry, Nanchang University, Nanchang 330031, P. R. China. E-mail: chaochen@ncu.edu.cn; hongsanguo2020@163.com*

[b]*Key Laboratory of Organo-Pharmaceutical Chemistry of Jiangxi Province, College of Chemistry and Chemical Engineering, Gannan Normal University, Ganzhou 341000, P. R. China. E-mail: luoxuzhong@hotmail.com*

† Electronic supplementary information (ESI) available: Detailed synthetic procedures, FT-IR, LC-MS, ^{1}H and ^{13}C NMR spectra of all compounds, the measurement results of gelation property, plots of MGC, single crystal X-ray diffraction data (CCDC 2034932), DSC curves and schematic of the mechanism, Tables S1–S7, and Fig. S1–S4. CCDC 2034932. For ESI and crystallographic data in CIF or other electronic format see DOI: 10.1039/d1ra00647a

‡ These authors contributed equally to this work.

assembly, molecular packing tuned by building unit structure and assembly strategies ultimately determined the corresponding devices' electronic properties.[10] Feng's team evaluated the influence of solvent viscosity, polarity and molecular size on the organogel properties and aggregate structures of methyl 4,6-*O*-(*p*-chlorobenzylidene)-α-D-glucopyranoside (MPBG) in different solvents. The result indicated that solvent viscosity acted as a key role in determining morphologies of aggregates.[11] Würthner and coworkers discovered that an achiral perylene bisimide derivative in *R*- or *S*-limonene could separately self-assemble into left- (*M*) and right-handed (*P*) helices at dilute state with an enantiomeric excess close to 100% on account of the chirality induction. Whereas, the enantiomeric excess of only about 20% was obtained at relatively high concentration, which might be attributed to the competing kinetic and thermodynamic self-assembly pathways.[12] Water is the most common solvent widely used in solvent-mediated strategies, no matter miscible or immiscible with organic solvents. For instance, Kim's team described the solvent dependent generation of microfibers, gels and hollow spheres from an azobenzene-containing benzenetricarboxamide derivative in aqueous-organic solvent systems for DMSO, DMF and THF, respectively. A reversible, fiber-to-sphere morphological transition was observed upon exposure to aqueous THF or pure DMSO, implying that the self-assemblies have potential applications in supramolecular memory materials.[13] The triggering effect of water in organogelation and tuning self-assembled nanostructures as well as the supramolecular chirality of a cationic amphiphile containing pyridinium was demonstrated in detail by Liu and coworkers.[14] Hao' group investigated the self-assembly behavior of an *N*-fluorenyl-9-methoxycarbonyl-based molecule in H_2O–DMSO system. By changing the water fraction, the switching on and off of chirality amplification was achieved successfully during self-assembly process.[15] Although water-mediated self-assembly have been reported by numerous literatures, interactions between the solvent and the solute are still relatively unclear.

Supramolecular hydrogels fabricated from molecular self-assembly of low-molecular-weight gelators (LMWGs) are well known for their potential applications in biomedicine,[16] drug delivery,[17] catalysis,[18] chemical sensors,[19] materials synthesis,[20] environmental remediation,[21] *etc.*[22] The gelation and crystallization of LMWGs are two closely related types of non-equilibrium self-assembly processes; both take place in oversaturated solutions and undergo nucleation and growth processes.[23] Focusing on the properties of supramolecular gels and the transformation of gel to crystal, notably the corresponding LMWG crystal structure, is a good strategy for clarifying the interactions between solvents and solutes in water-mediated self-assembly processes. Dastidar' group developed a pyridyl urea-based low molecular weight supramolecular hydrogelator, which could be crystallized from its gelling H_2O–EG system for the first time. Analysis of the single crystal structure indicated that the bonding sites of the gelator molecule are fully filled by various hydrogen bonds formed with the solvent molecules.[24] By common microscopic methods, a pentapeptide gel–crystal phase transition amenable for continuous visualization and quantification was presented by Gazit and co-workers. The transition kinetics and crystal morphology modulated by extrinsic factors, such as temperature, solvent composition and mechanical perturbation, was also demonstrated.[25] Inspired by previous excellent achievements, our group has reported a thermo-sensitive supramolecular hydrogel derived from an onium salt TTIBD with solution–gel–crystal transition properties. The step-wise gel-to-crystal transformation, also being an amorphous-to-crystalline phase transition process, was observed upon extension of the aging time.[26] Pyridinedicarboxylic acids are a type of building blocks to fabricate gelators due to their easy chemical modification and biocompatibility. Therefore, the design and functional application for derivatives containing pyridinedicarboxylic acid groups is a research field worth exploring.

Herein, 3,5-pyridinedicarboxylic acid-based compounds (*N*,*N*′-di(pyridin-4-yl)-pyridine-3,5-dicarboxamide, PDA-N4; *N*,*N*′-di(phenyl)-pyridine-3,5-dicarboxamide, PDA-Ph; *N*,*N*′-di(pyridin-4-yl)-pyridine-3,5-dicarbomethoxy, PDA-O4) were designed and used to construct supramolecular self-assemblies *via* a solvent-mediated strategy under mild conditions. Their gelation properties with changes in the water content of mixed solvents were investigated. The microstructure and morphology of aggregates were observed. The solution–gel–crystal transition behaviors, mechanical properties, pH- and thermo-reversibility of supramolecular gels were also explored. Moreover, the molecular arrangement of gelators in single crystals was analyzed, and then the possible self-assembly mechanism in gels was further proposed. Additionally, the human umbilical venous endothelial cell (HUVEC) culture and the controlled drug delivery of vitamin B12 (VB_{12}) were investigated.

2. Experimental section

2.1 Materials

Analytical grade pyridine-3,5-dicarboxylic acid and 4-aminopyridine were purchased from J&K Scientific Co., Ltd. (Shanghai, China). Analytical grade 4-hydroxypyridine and 3-aminopyridine were obtained from Adamas Reagent, Ltd. (Shanghai, China). Analytical grade VB_{12}, NaOH, HCl, Na_2HPO_4, KH_2PO_4 and citric acid were purchased from Innochem Technology Co., Ltd. (Beijing, China). Analytical grade thionyl chloride ($SOCl_2$), dimethyl sulfoxide (DMSO) and *N*,*N*-dimethylformamide (DMF) were purchased from Aladdin Chemical Reagent Co., Ltd. (Shanghai, China). All other organic solvents were obtained from Tianjin Damao Chemical Reagent Factory (Tianjin, China). All experiments were performed by using deionized water. Phosphate buffer solutions (PBS, pH = 10.0 and 7.4) were prepared by a standard method.

2.2 Synthesis and gelation test

All derivatives of 3,5-pyridinedicarboxylic acid (PDA-N4, PDA-Ph and PDA-O4) were prepared according to the literature method,[27] and then characterized by FT-IR, ^{1}H NMR, ^{13}C NMR and LC-MS, respectively (Scheme S1, ESI†). Their gelation ability in various solutions was investigated by the typical 'inversion test'.[26,28] For the test, a certain amount of sample was dissolved

into an organic solvent under ultrasound. Subsequently, the solution was immediately mixed with deionized water in a vial at room temperature. After standing for 5 min, the vial was turned upside down, in which the viscoelastic mixture that did not fall down could be defined as a gel. The corresponding xerogels were obtained by freeze-drying technology.

2.3 Characterization

Scanning electron microscope (SEM) images were captured by a FEI Quanta 450 SEM. Differential scanning calorimetry (DSC) heating curves were acquired by a Setaram μDSC7-Evo instrument (heating rate, 1.0 °C min^{-1}). ^1H NMR spectra were obtained by using a Bruker AM400 spectrometer. Powder X-ray diffraction (PXRD) patterns were recorded on a Bruker D8 Focus diffractometer with Cu-Kα radiation (λ = 1.5418 Å). Single-crystal X-ray diffraction (SCXRD) data were collected on a Bruker Smart APEX II diffractometer. Fourier transform infrared (FT-IR) spectra were recorded by using a Nicolet AVATAR 360 spectrometer in the region between 4000 and 400 cm^{-1} at 4 cm^{-1} spectral resolution. Mass spectra were collected on a Bruker Dalton Esquire 3000 plus LC-MS apparatus. Rheological data were obtained by a HAAKE RheoStress 6000 stress-controlled rheometer with parallel plate type geometry (plate diameter, 3.5 cm). Ultraviolet-visible (UV-vis) absorption spectra were recorded by using a Shimadzu UV-1800 spectrophotometer. Cell viability was observed under a Leica DMIRB inverted fluorescence microscope.

2.4 Controlled release of VB_{12}

A certain amount of PDA-N4 and VB_{12} were dissolved into a specific organic solvent. Subsequently, the organic solution was transferred into a glass-stoppered test tube containing fresh PBS with a defined pH, forming stable gel (PBS/organic solvent = 9, v/v). After that, 8 mL of PBS with same pH used as VB_{12} receiving media was carefully transferred to top of the hydrogel. Finally, the release equilibrium process was investigated. At a scheduled interval, 2 mL of the supernatant was extracted to determine the VB_{12} concentration released from PDA-N4 gel by UV-vis spectrometry. Meanwhile, an equal volume of fresh PBS was added to the buffer system for maintaining balance. All tests were performed in triplicate unless otherwise specified.

2.5 2D cell culture

Before cell seeding, each well in 96-well plate was coated with dried PDA-N4 gel film and sterilized under UV-irradiation system for 30 min. After trypsinized with pancreatic enzymes and centrifuged at 1000 rpm for 5 min, the cells were resuspended and diluted by DMEM (counted by using a hemocytometer). Subsequently, they were transfered into the coated 96-well plate in sextuplicate with 100 μL per well (1000 cells per well). At a scheduled time point (4 h), the media was removed. And then each well was washed with PBS twice, followed by addition of 100 μL DMEM (containing 10% fetal calf serum). Finally, the 96-well plate was placed in incubator with 5% CO_2 at 37 °C. The cultured cells were stained by calcein-AM and imaged by inverted fluorescence microscope. The cell viability was evaluated *via* CCK-8 method.

3. Results and discussion

3.1 Gelation properties

The gelation ability of PDA-N4 in a series of organic solvents and H_2O was systematically investigated *via* the typical 'inversion test' method. It was found that PDA-N4 could be dissolved easily in some strong polar organic solvents including DMSO, DMF, methanol, ethanol and 1,4-dioxane to form a clear solution. However, it was difficult to dissolve in non- or weak-polar solvents such as benzene, carbon tetrachloride and tetrahydrofuran. In the organic solvents used in this work or water, no gel of PDA-N4 could be formed (Table S1†). Surprisingly, adding water into a DMSO/DMF solution of PDA-N4 to a certain amount, the solution could transform into gels finally. Keeping the PDA-N4 concentration constant at 15 mg mL^{-1}, a solution–suspension–gel transition was observed as the water content (volume ration, vol%) in H_2O–DMSO mixed solvent increased in the range of 0% to 90%. This phenomenon suggests that water induces the self-assembly of PDA-N4 molecules in solution. More detailed results are shown in Scheme 1 and Table S2.† As displayed in Scheme 1, a stable white gel can be formed instantly with water content greater than or equal to 50%. Moreover, the obtained gel is thermo-reversible. Heating the gel, it gradually transforms into clear solution, and more uniform gel will be formed again after cooling to room temperature. It should be noted that the PDA-N4 gel (water content = 50%) and suspension, as well as the solution (water content > 25%) could transform into crystal after standing for a certain time at room temperature, while only transparent solution (water content < 25%) even for a longer time. In addition, the transition process is also thermo-reversible (Fig. 1). The conversion time for solution (water content = 30%) requires about 1 day, while near 5 days for the suspension. The stable periods for PDA-N4 gels varied with the concentration and water content are summarized in Table S3.† As illustrated in Table S3,† a prominent extension is observed upon increasing the water content or PDA-N4 concentration. For example, the stable periods for PDA-N4 gels (15 mg mL^{-1}) formed in 50% and 80% aqueous systems are 10 and more than 90 days, respectively.

The minimum gelator concentrations (MGC) for PDA-N4 gelation in mixed solvents were also investigated (Fig. S1†). It decreases as the water content increases. The MGC in aqueous systems of 50%, 80% and 90% are 15, 11 and 9 mg mL^{-1}, respectively. Moreover, the gels formed in aqueous systems with the water content greater than or equal to 80% could exist stably for more than 90 days (Table S3†). In this work, the pH effect on PDA-N4 gelation was also evaluated. As shown in Fig. S2,† the white gel is stable when solution pH is greater than 5. It would be broken down gradually after adjusting solution pH to lower than 4 by adding 0.1 M HCl, and then transform into a clear solution finally at pH 2. Whereas, a stable gel could be observed again with the solution pH adjusted to more than 5 by adding 0.1 M NaOH. Moreover, this process is repeatable, revealing that

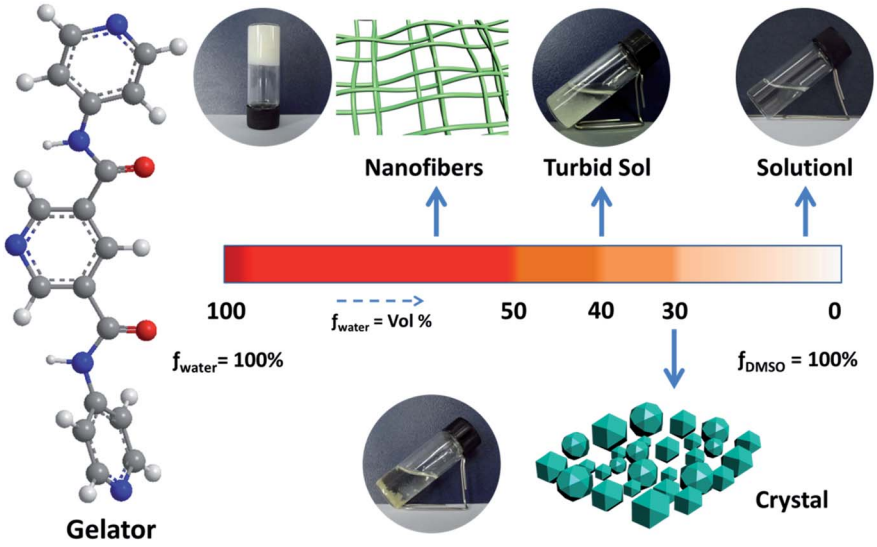

Scheme 1 Molecular structure of PDA-N4 (marked as gelator) and schematic diagram of the phase transition with water content in H_2O–DMSO mixed solvent at a constant PDA-N4 concentration ($c_{PDA\text{-}N4}$ = 15 mg mL^{-1}).

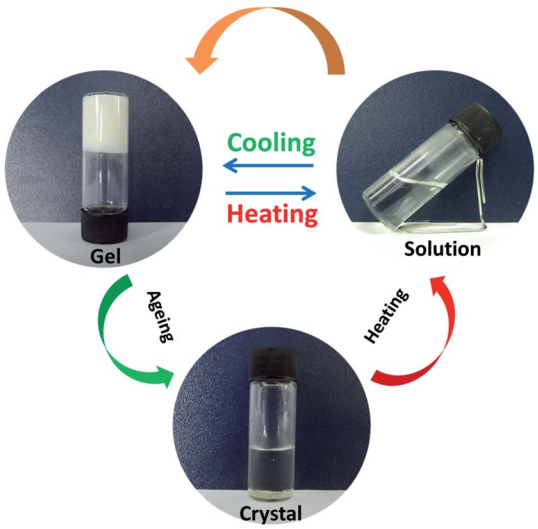

Fig. 1 Schematic diagram of the reversible solution–gel–crystal transition process (DMSO–H_2O = 1 : 1, v/v; $c_{PDA\text{-}N4}$ = 15 mg mL^{-1}).

the PDA-N4 gels formed in DMSO–H_2O mixed solvent are pH-responsive.

Similar results were also found in the gelation process of PDA-N4 in DMF–H_2O mixed solvents (Table S4†). However, no gel formation could be observed in methanol–H_2O, ethanol–H_2O and 1,4-dioxane–H_2O mixed systems (Table S5–S7†). In order to obtain insights into the relationship between chemical structures and gelation properties, compounds PDA-Ph (4-aminopyridine replaced by aniline) and PDA-O4 (4-aminopyridine replaced by 4-hydroxypyridine) were also synthesized (Scheme S1, ESI†). Unfortunately, no gelation was observed for PDA-Ph and PDA-O4 in selected liquids (Tables S1, S2 and S4–S7†). This result indicates that the gelation abilities of gelators strongly depend on their molecular structures. Compared with PDA-N4, PDA-O4 has less H-bond donors, and PDA-Ph exhibits fewer H-bond acceptors. Therefore, the existing H-bonding is not enough for molecular gelation.

3.2 Morphology and microstructure

To investigate the variation in morphology and microstructure, the xerogels of PDA-N4 were characterized visually by SEM. As shown in Fig. 2a, the aggregates of gelator molecules exhibit fibrous structure (width: 0.1–0.2 μm) in DMSO–H_2O mixed system with 90% water content. When the water content was decreased to 50%, the fibers become wider (width: 0.15–0.8 μm, Fig. 2b). This result indicates that the PDA-N4 gels are composed of a 3D self-assembly network of fibers and entrapped liquids. During the experiment, short gelation time suggests a kinetically controlled growth of 1D fiber. By decreasing the water content, molecular aggregates may favor other dimensional growth as well, weakening the surface tension and capillary forces, and finally giving rise to the instability of the gel (relatively short gel–crystal transition time, Table S3†).[14,29] A similar result was also observed in the DSC analyses (Fig. S3†). In addition, the gel–crystal transition process upon extension of the aging time was also investigated by SEM. As shown in Fig. 2c, some granular crystals together with fibrous structures appear in the gel aged at room temperature for 10 days. The appearance of granular crystals makes the 3D network less effective to entangle the solvent, which leads to the destruction of gel. When the gel was aged for 30 days, bulk crystals were eventually generated (Fig. 2d). As previous reports have clarified, the gelation and crystallization are orthogonal and time-resolved processes under non-equilibrium conditions.[30] Crystallization occurs over a period of hours to days due to the presence of an unfavorable nucleation step, but gelation often take place at a shorter time interval.[31] Therefore, during the supramolecular self-assembly process, gelators in suitable solvents are firstly trapped in kinetically favorable gel state, and

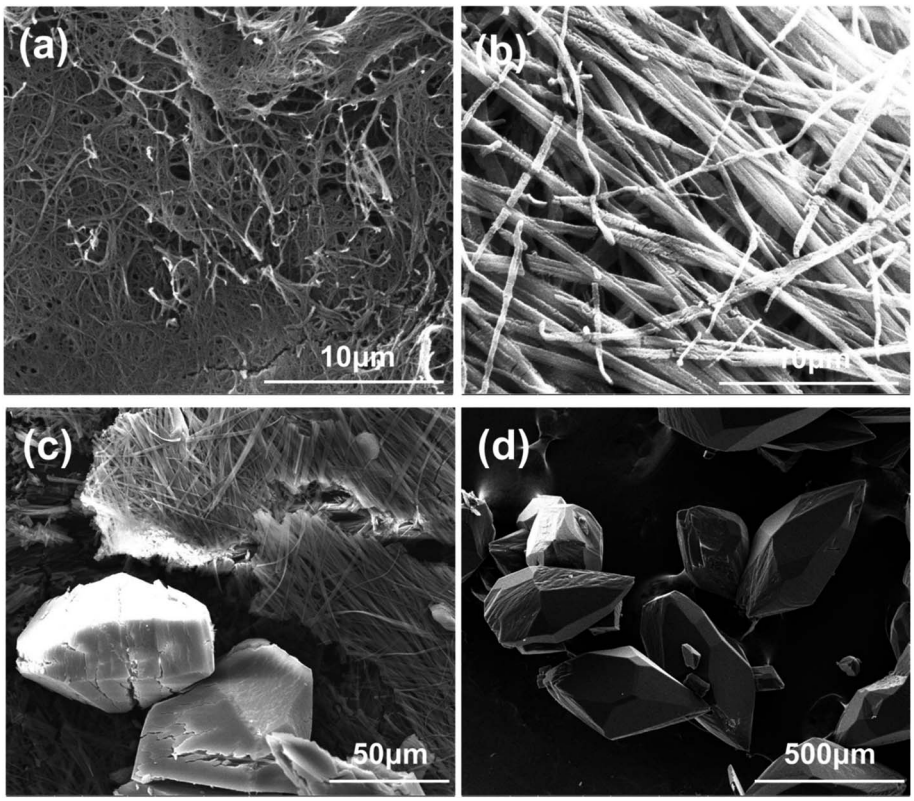

Fig. 2 SEM images of the PDA-N4 aggregates in DMSO–H_2O mixed system ($c_{PDA\text{-}N4}$ = 15 mg mL^{-1}) with (a) 90% and (b) 50% water contents; SEM images of the PDA-N4 xerogels (formed in DMSO–H_2O mixed system with 50% water content) aged at room temperature for (c) 10 and (d) 30 days.

then transfer into a more thermodynamically stable crystal state upon ageing.[32]

3.3 Rheological properties

The mechanical properties of materials are extremely important for their practical applications, so rheological measurements were employed to investigate the viscoelastic properties of PDA-N4 gels. As displayed in Fig. 3, all gels exhibit a higher elastic storage modulus (G') and a lower loss modulus (G''), demonstrating the authenticity of gelation judgment.[33] As illustrated in Fig. 3a, the values of G' and G'' remain almost constant when the shear stress is less than the critical shear stress, which implies that the structure of PDA-N4 gel is completely intact. Thereafter, the collapse of gel network appears, as proved by a dramatic decrease in the values of both modulus and the reversal of viscoelastic signal. Moreover, both G' and G'' increase gradually with the increasing water content from 50% to 90% (Fig. 3a–c), indicating the enhancement of mechanical properties. The dynamic frequency sweep measurement was employed to confirm the elastic behavior of PDA-N4 gel. As depicted in Fig. 3a′–c′, the value of G' is greater than that of G'', and both modulus exhibit slight frequency dependence from 0.1 to 100 rad s^{-1}, revealing the typical viscoelastic feature of supramolecular gels.

3.4 Self-assembly mechanism

Crystallography data could provide an opportunity to understand the role of various non-covalent interactions in the formation of supramolecular self-assemblies. To get insight into how molecules self-assemble in crystals and the relationship between gelation and crystallization, the molecular arrangement of PDA-N4 in single crystals was investigated by SCXRD. The same unit cell parameters indicate that the crystals obtained from the saturated solution are of the same type as those transformed from PDA-N4 gels. As shown in Table S8 (ESI†), PDA-N4 crystallizes in the monoclinic space group $P2_1/c$ with lattice parameters a = 14.6401(3) (Å), b = 8.4503(2) (Å), c = 13.3398(3) (Å) and $\alpha = 90°$, $\beta = 112.159(3)°$, $\gamma = 90°$. The hydrogen bond geometry, selected bond lengths and angles are listed in Tables S9 and S10 (ESI†), respectively. Further structure information has been deposited at the Cambridge Crystallographic Data Centre (CCDC 2034932†). The asymmetric unit is composed of one PDA-N4 molecule and one water molecule. As depicted in Fig. 4a, adjacent PDA-N4 molecules are connected to each other by N(6)–H(6)···N(5) hydrogen bonding, in which the imino of amide donates a H atom to the pyridyl N atom. Meanwhile, one water molecule is linked with two PDA-N4 molecules *via* N(3)–H(3)···O(2) and O(2)–H(2)···N(2) hydrogen bonding. In addition, π–π stacking interactions exist between the adjacent pyridine rings of PDA-N4 molecules, creating a three-dimensional (3D) structure finally (Fig. 4b).

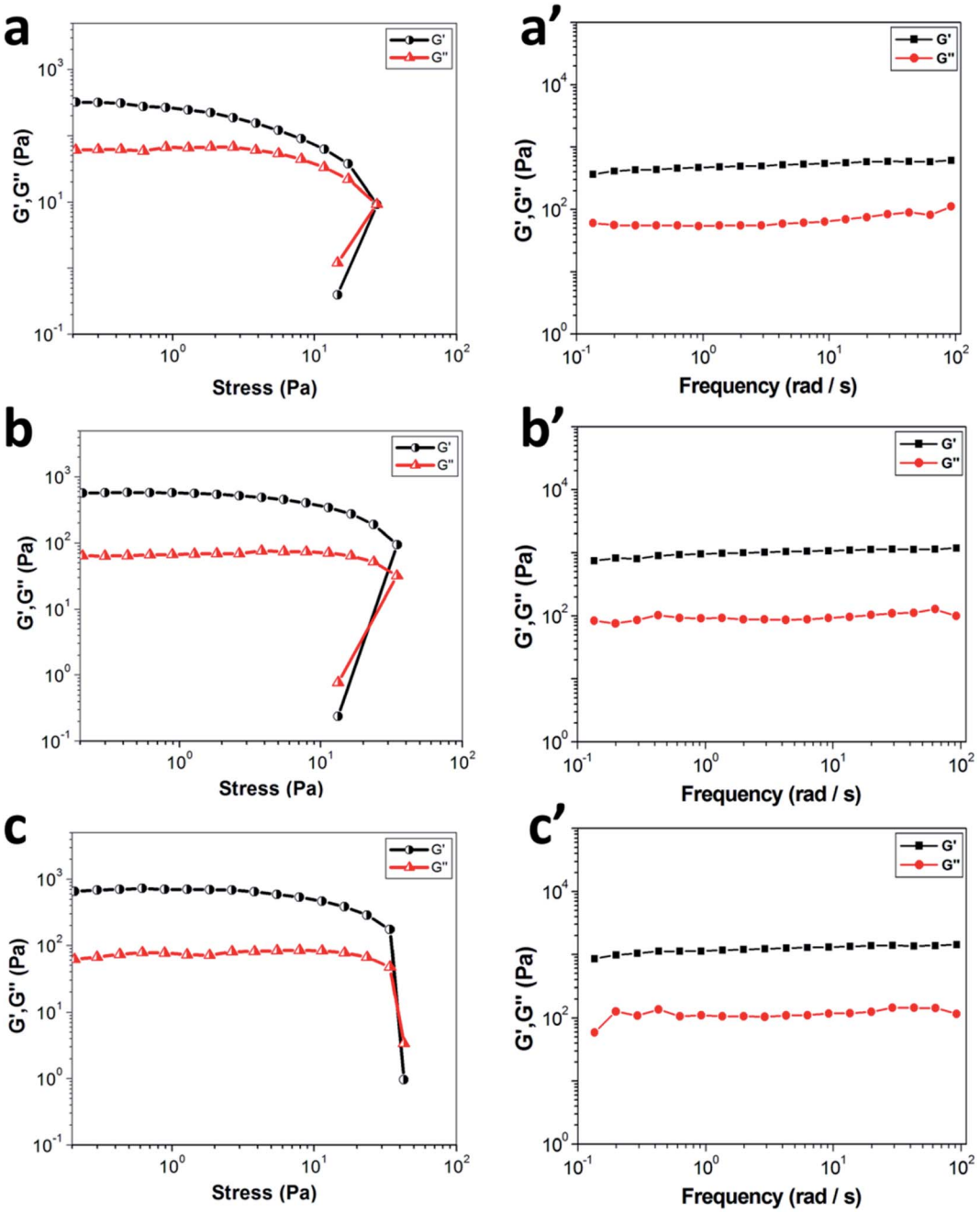

Fig. 3 Rheological behavior of PDA-N4 gels formed in DMSO-H_2O mixed systems with (a and a′) 50%, (b and b′) 70% and (c and c′) 90% water contents (a, b and c are strain sweep modes; a′, b′ and c′ are frequency sweep modes at a constant stress of 1 Pa).

FT-IR technology has been widely used to investigate intermolecular hydrogen bonding interactions. As can be appreciated in Fig. 5a, the FT-IR spectrum of PDA-N4 crystals is characterized by peaks appearing at 1679 and 3242 cm^{-1}, which could be attributed to the νC=O and νN–H of amide groups, respectively. Compared with the N–H stretching vibration (3440 cm^{-1}) of the free secondary amide group, a red shift is observed for that of PDA-N4 crystals, implying the formation of strong hydrogen-bonding interactions between adjacent molecules. However, there is no obvious shift for C=O stretching vibration (free state: 1680 cm^{-1}), indicating that the C=O group does not take part in the construction of hydrogen-bonding.[34] Similar results are also obtained for the PDA-N4 gels with different solvent rations, suggesting that the analogical intermolecular hydrogen bonding appears in PDA-N4 gels and crystals.

To provide further evidence for the intermolecular interactions, ^{1}H NMR technique was used to investigate the self-assembly process of gelation. In general, ^{1}H NMR signals of molecules in solution are sharp at suitable field strengths, while

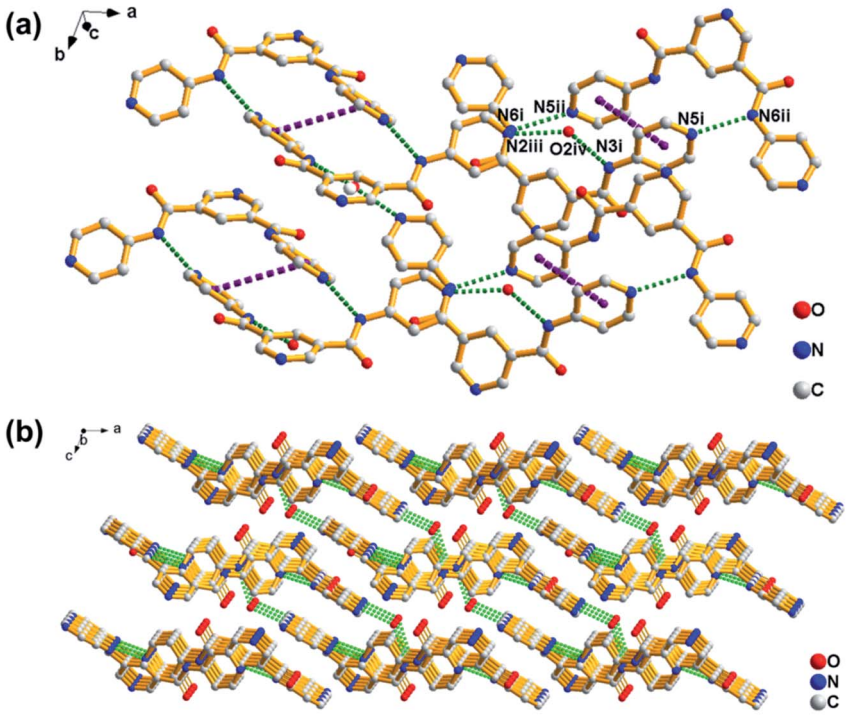

Fig. 4 Intermolecular bonding (a) and 3D structure (b) of PDA-N4 crystals (green and purple dashed lines indicate hydrogen bonds and π–π stacking interactions, respectively. Symmetric codes: (i) = −1 + *x*, −1 + *y*, −1 + *z*; (ii) = 1 − *x*, −1 − *y*, −*z*; (iii) = −*x*, −0.5 + *y*, −0.5 − *z*; (iv) = −1 + *x*, −0.5 − *y*, −1.5 + *z*).

those in liquid crystal, glass and gel phases broaden and exhibit a specific shift. Fig. 5b presents the ^{1}H NMR spectra of PDA-N4 in various DMSO-*d*6–D_2O mixed systems ($c_{PDA\text{-}N4}$ = 15 mg mL^{-1}). It can be observed that the aromatic proton signals for PDA-N4 in solution phase (DMSO-*d*6 as solvent) are well-dispersed and appear at 9.30 (d, H_a), 8.83 (t, H_b) 8.58–8.45 (m, H_c) and 7.79 ppm (dd, H_d). By increasing the water content from 10% to 40%, the signals gradually become broad, insensitive and even shift upfield, indicating that π–π stacking interaction promotes the self-assembly process. When the water content reaches 50%, they are even more inconspicuous, implying the gelation of PDA-N4.[35]

Additionally, PXRD patterns were also acquired in order to determine the structure. As shown in Fig. 5c, the intensity of diffraction peaks for xerogels gradually weakened with the increase of water content in mixed systems, implying a decreasing degree of molecular stacking in gelation. However, the diffraction peaks for PDA-N4 xerogels at 2θ = 12.3°, 13.0°, 14.1°, 16.1°, 16.7°, 17.6°, 21.0°, 22.3° and 26.3° are always consistent with those of crystals, indicating that both the corresponding gel and crystal have similar assembly structures. In brief, the molecular assembly in PDA-N4 gels depends on intermolecular π–π stacking interaction and hydrogen bonds, as proved by the crystal structure and spectrum analysis. By introducing water, gelator molecules tended to aggregate to form fibers, further generating a 3D network in which abundant liquid in the interspaces is immobilized (Fig. S3†).

3.5 Release behavior of PDA-N4 gels

In recent years, various supramolecular hydrogels have exhibited potential biomedical applications, such as controlled drug delivery, cell culture and tissue engineering.[36] Herein, VB_{12} as a water-soluble and UV-active model drug was employed to investigate the controlled drug release behavior of PDA-N4 gels. In the experiment, VB_{12} could be trapped in gels without disturbing the gelation ability of PDA-N4. The corresponding release kinetics is shown in Fig. 6. As can be observed from Fig. 6a, the accumulative release percentage of VB_{12} gradually increases over time. Moreover, it also increases with the increase of VB_{12} concentration from 140 mg L^{-1} to 220 mg L^{-1}. However, the release rate displays a decreasing trend and reaches an equilibrium process finally. In addition, the sustained-release data were fitted by the typical first-order kinetic model ($M_t/M_\infty = 1 - \exp(-k \times t)$, where M_t denotes the amount of drug released at time t, M_∞ refers to the maximal amount of drug at infinite time, and k is the rate constant).[37] As displayed in Fig. 6b, an excellent linear correlation is obtained. The correlation coefficients for VB12 at different initial concentrations (140, 180 and 220 mg L^{-1}) are 0.9885, 0.9881 and 0.9933, respectively. Clearly, the release behavior of VB12 from PDA-N4 gels is in accordance with the first-order kinetic mechanism.

3.6 Bio-compatibility of PDA-N4

In order to investigate the bio-compatibility of PDA-N4, its cyto-compatibility *in vitro* was evaluated by 2D culture of HUVECs. The fluorescence microscopy images of HUVECs after

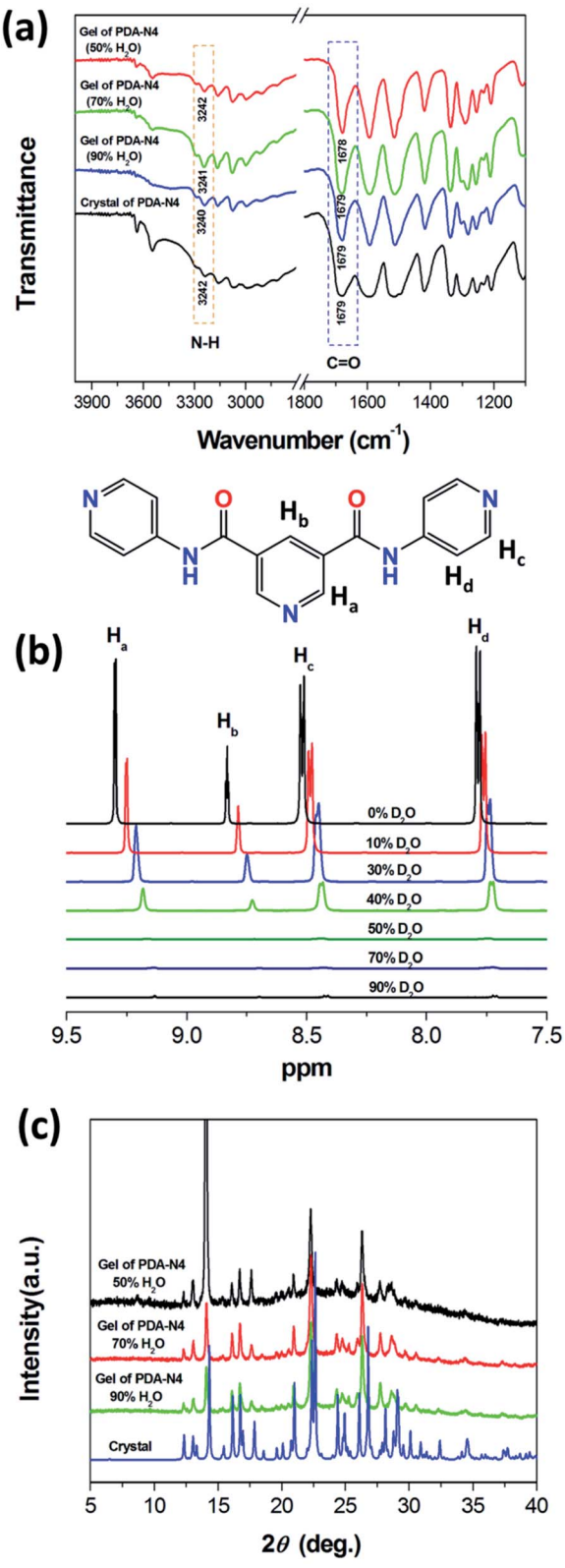

Fig. 5 (a) FT-IR spectra of the PDA-N4 crystals and xerogels, (b) ^{1}H NMR spectra of PDA-N4 in various DMSO-*d*6–D_2O mixed systems, and (c) PXRD patterns of the PDA-N4 crystals and xerogels ($c_{PDA\text{-}N4}$ = 15 mg mL^{-1}).

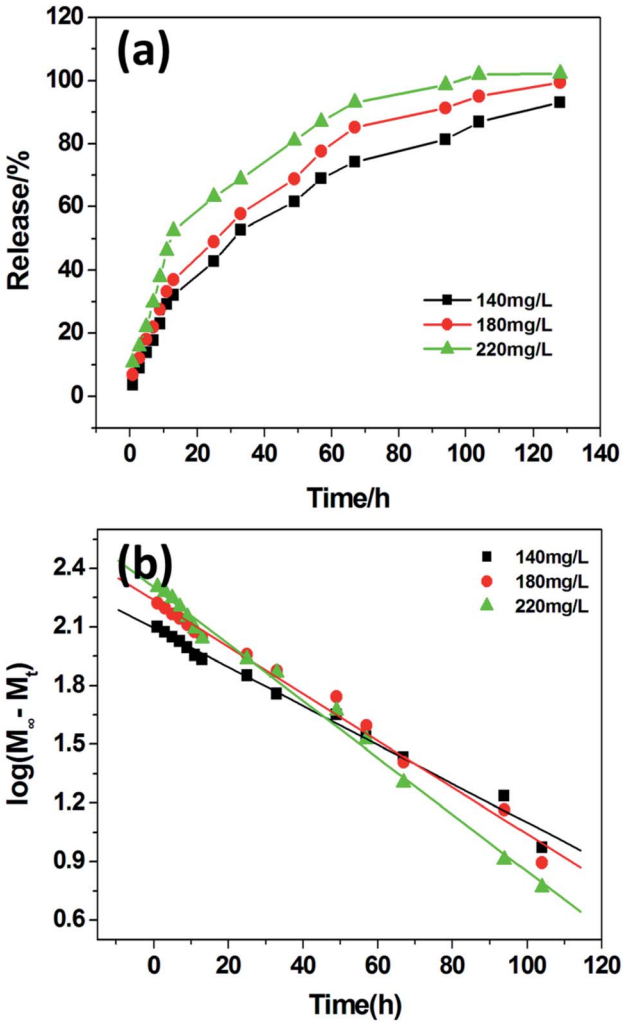

Fig. 6 (a) Effect of the VB_{12} concentration on drug release in PDA-N4 hydrogels (water content = 90%) at room temperature and (b) the corresponding kinetics profiles with given time ($c_{PDA\text{-}N4}$ = 15 mg mL^{-1}, pH = 7.4).

incubation at different culture periods were recorded. As presented in Fig. 7, the cell density distribution of HUVECs is significantly heightened upon extension of the culture period. After cultivation for 1 day (Fig. 7a), rounded HUVECs adhered over samples can be observed clearly. When the cultivation period reaches 3 days (Fig. 7b), some cells exhibit an elliptical shape in pairs, indicating that the HUVECs are subjected to cell division. By extending the cultivation period from 3 to 7 days, the cell density distribution increases gradually (Fig. 7c and d). Similar phenomenon was also observed in previous reports.[38] In addition, the proliferation of HUVECs was quantitatively evaluated by using the prestoblue assay (colorimetric method). As shown in Fig. 7e, the number of living cells per mL is obviously increased upon prolonging cultivation periods. Moreover, the average number of HUVECs cultivated for 7 days is approximately 6 times that for 1 day. These results indicate the good bio-compatibility of PDA-N4.

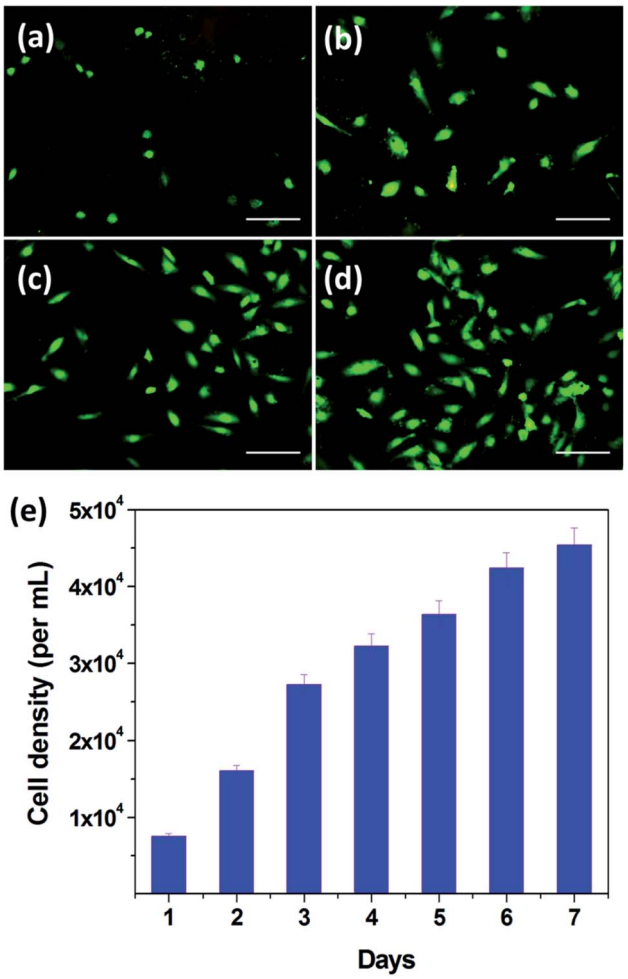

Fig. 7 Fluorescence microscopy images of HUVECs after incubation for (a) 1 day, (b) 3 days, (c) 5 days and (d) 7 days (scale bar: 100 μm, cell seeding density: 1.0 × 10^4 cells per mL); (e) the density of HUVECs at different culture periods.

4. Conclusion

In summary, we have designed three derivatives containing pyridinedicarboxylic acid groups and investigated their supramolecular gelation *via* a solvent-mediated strategy under mild conditions. By adjusting the water content in mixed systems, the gel, suspension and solution phases for PDA-N4 were observed, respectively. Moreover, the PDA-N4 gels not only displayed solid-like behavior, pH- and thermo-reversible characteristics, but also showed a solution–gel–crystal transition upon extending the aging time. Both the crystal and gel had similar assembled structure, which was constructed by hydrogen bonding and π–π stacking interactions. Furthermore, the PDA-N4 exhibited good cyto-compatibility for HUVECs, and the corresponding gels presented controllable drug release for VB_{12}. The release process was in accordance with first-order release behavior. This research is expected to provide a new material for the cell culture and controlled drug release.

Conflicts of interest

There are no conflicts of interest to declare.

Acknowledgements

This work was financially supported by the National Natural Science Foundation of China (21663004, 21661020 and 21961021), Science and Technology Project of Jiangxi Provincial Department of Education (GJJ190774, GJJ201425 and GJJ201426) and Graduate Innovation Foundation of Nanchang University (cx2016012).

References

1 (*a*) J. Li, J. Wang, H. Li, N. Song, D. Wang and B. Z. Tang, *Chem. Soc. Rev.*, 2020, **49**, 1144–1172; (*b*) S. Mondal, S. Das and A. K. Nandi, *Soft Matter*, 2020, **16**, 1404–1454; (*c*) J. Gao, J. Zhan and Z. Yang, *Adv. Mater.*, 2019, 1805798; (*d*) P. W. J. M. Frederix, I. Patmanidis and S. J. Marrink, *Chem. Soc. Rev.*, 2018, **47**, 3470–3489; (*e*) N. Falcone and H. Kraatz, *Chem.–Eur. J.*, 2018, **24**, 1–14; (*f*) M. Liu, L. Zhang and T. Wang, *Chem. Rev.*, 2015, **115**, 7304–7397.

2 (*a*) R. Kuosmanen, K. Rissanen and E. Sievänen, *Chem. Soc. Rev.*, 2020, **49**, 1977–1998; (*b*) J. Zhong, H. Fu, X. Jia, H. Lou, T. Wan, H. Luo, H. Liu, D. Zhong and X. Luo, *RSC Adv.*, 2019, **9**, 11824–11832; (*c*) H. Cao, P. Duan, X. Zhu, J. Jiang and M. Liu, *Chem.–Eur. J.*, 2012, **18**, 5546–5550; (*d*) T. Bollhorst, K. Rezwan and M. Maas, *Chem. Soc. Rev.*, 2017, **46**, 2091–2126; (*e*) Y. Qiu, P. Chen and M. Liu, *J. Am. Chem. Soc.*, 2010, **132**, 9644–9652; (*f*) F. Wang and C. Feng, *Angew. Chem., Int. Ed.*, 2018, **57**, 5655–5659; (*g*) P. Choudhury, K. Das and P. K. Das, *Langmuir*, 2017, **33**, 4500–4510.

3 J. Cui, A. Liu, Y. Guan, J. Zheng, Z. Shen and X. Wan, *Langmuir*, 2010, **26**, 3615–3622.

4 Z. Sun, Z. Li, Y. He, R. Shen, L. Deng, M. Yang, Y. Liang and Y. Zhang, *J. Am. Chem. Soc.*, 2013, **135**, 13379–13386.

5 (*a*) D. Núñez-Villanueva, M. A. Jinks, J. G. Magentia and C. A. Hunter, *Chem. Commun.*, 2018, **54**, 10874–10877; (*b*) N. Komiya, T. Muraoka, M. Iida, M. Miyanaga, K. Takahashi and T. Naota, *J. Am. Chem. Soc.*, 2011, **133**, 16054–16061.

6 (*a*) G. Ghosh, R. Barman, J. Sarkar and S. Ghosh, *J. Phys. Chem. B*, 2019, **123**, 5909–5915; (*b*) I. Willner, *Acc. Chem. Res.*, 2017, **50**, 657–658.

7 (*a*) P. Xing, C. Yang, Y. Wang, S. Z. F. Phua and Y. Zhao, *Adv. Funct. Mater.*, 2018, 1802859; (*b*) W. Edwards, C. A. Lagadec and D. K. Smith, *Soft Matter*, 2011, **7**, 110–117; (*c*) V. Caplar, L. Frkanec, N. S. Vujicic and M. Zinic, *Chem.–Eur. J.*, 2010, **16**, 3066–3082; (*d*) J. Cui, J. Zheng, W. Qiao and X. Wan, *J. Colloid Interface Sci.*, 2008, **326**, 267–274.

8 (*a*) L. Zhang, L. Qin, X. Wang, H. Cao and M. Liu, *Adv. Mater.*, 2014, **26**, 6959–6964; (*b*) S. Xue, P. Xing, J. Zhan, Y. Zeng and Y. Zhao, *Chem.–Eur. J.*, 2018, **25**, 7426–7437.

9 (*a*) E. Rabani, D. R. Reichman, P. L. Geissler and L. E. Brus, *Nature*, 2013, **426**, 271–274; (*b*) P. Jonkheijm, P. van der

Schoot, A. P. H. J. Schenning and E. W. Meijer, *Science*, 2006, **313**, 80–84; (*c*) Y. Mao, K. Liu, L. Meng, L. Chen, L. Chen and T. Yi, *Soft Matter*, 2014, **10**, 7615–7622; (*d*) J. H. Ortony, B. Qiao, C. J. Newcomb, T. J. Keller, L. C. Palmer, E. Deiss-Yehiely, M. O. de la Cruz, S. Han and S. I. Stupp, *J. Am. Chem. Soc.*, 2017, **139**, 8915–8921; (*e*) Q. Jin, L. Zhang and M. Liu, *Chem.–Eur. J.*, 2013, **19**, 9234–9241.

10 Y. Sun, C. He, K. Sun, Y. Li, H. Dong, Z. Wang and Z. Li, *Langmuir*, 2011, **27**, 11363–11371.

11 H. Xu, J. Song, T. Tian and R. Feng, *Soft Matter*, 2012, **8**, 3478–3486.

12 V. Stepanenko, X. Q. Li, J. Gershberg and F. Würthner, *Chem. Eur. J.*, 2013, **19**, 4176–4183.

13 S. Lee, S. Oh, J. Lee, Y. Malpani, Y. Jung, B. Kang, J. Lee, K. Ozasa, T. Isoshima, S. Lee, M. Hara, D. Hashizume and J. Kim, *Langmuir*, 2013, **29**, 5869–5877.

14 C. Liu, Q. Jin, K. Lv, L. Zhang and M. Liu, *Chem. Commun.*, 2014, **50**, 3702–3705.

15 Y. Zhang, S. Li, M. Ma, M. Yang, Y. Wang, A. Hao and P. Xing, *New J. Chem.*, 2016, **40**, 5568–5576.

16 R. Parveen, B. Jayamma and P. Dastidar, *ACS Biomater. Sci. Eng.*, 2019, **5**, 2180–2189.

17 (*a*) M. J. Webber and R. Langer, *Chem. Soc. Rev.*, 2017, **46**, 6600–6620; (*b*) K. J. Skilling, F. Citossi, T. D. Bradshaw, M. Ashford, B. Kellama and M. Marlow, *Soft Matter*, 2014, **10**, 237–256.

18 F. Trausel, F. Versluis, C. Maity, J. M. Poolman, M. Lovrak, J. H. van Esch and R. Eelkema, *Acc. Chem. Res.*, 2016, **49**, 1440–1447.

19 F. Qu, Y. Zhang, A. Rasooly and M. Yang, *Anal. Chem.*, 2014, **86**, 973–976.

20 (*a*) S. Kiyonaka, K. Sada, I. Yoshimura, S. Shinkai, N. Kato and I. Hamachi, *Nat. Mater.*, 2003, **3**, 58–64; (*b*) S. Bera and D. Haldar, *J. Mater. Chem. A*, 2016, **4**, 6933–6939.

21 (*a*) B. O. Okesola and D. K. Smith, *Chem. Soc. Rev.*, 2016, **45**, 4226–4251; (*b*) B. Adhikari, G. Palui and A. Banerjee, *Soft Matter*, 2009, **5**, 3452–3460.

22 (*a*) A. M. Vibhute, V. Muvvala and K. M. Sureshan, *Angew. Chem., Int. Ed.*, 2016, **55**, 7782–7785; (*b*) C. D. Jones and J. W. Steed, *Chem. Soc. Rev.*, 2016, **45**, 6546–6596.

23 (*a*) L. Li, J. M. Scheiger and P. A. Levkin, *Adv. Mater.*, 2019, 1807333; (*b*) J. Mayr, C. Saldías and D. D. Díaz, *Chem. Soc. Rev.*, 2018, **47**, 1484–1515; (*c*) X. Du, J. Zhou, J. Shi and B. Xu, *Chem. Rev.*, 2015, **115**, 13165–13307.

24 D. K. Kumar, D. A. Jose, A. Das and P. Dastidar, *Chem. Commun.*, 2005, **32**, 4059–4061.

25 T. Guterman, M. Levin, S. Kolusheva, D. Levy, N. Noor, Y. Roichman and E. Gazit, *Angew. Chem., Int. Ed.*, 2019, **58**, 15869–15875.

26 X. Jia, J. Wang, D. Zhong, J. Wu, B. Zhao, D. den Engelsena and X. Luo, *RSC Adv.*, 2016, **6**, 109425–109433.

27 X. Z. Luo, X. J. Jia, J. H. Deng, J. L. Zhong, H. J. Liu, K. J. Wang and D. C. Zhong, *J. Am. Chem. Soc.*, 2013, **135**(32), 11684–11687.

28 (*a*) L. Liao, X. Zhong, X. Jia, C. Liao, J. Zhong, S. Ding, C. Chen, S. Hong and X. Luo, *RSC Adv.*, 2020, **10**, 29129–29138; (*b*) D. Zhong, L. Liao, K. Wang, H. Liu and X. Luo, *Soft Matter*, 2015, **11**, 6386–6392.

29 A. Vidyasagar and K. M. Sureshan, *Angew. Chem., Int. Ed.*, 2015, **54**, 12078–12082.

30 (*a*) D. Braga, S. d'Agostino, E. D'Amen and F. Grepioni, *Chem. Commun.*, 2011, **47**, 5154–5156; (*b*) D. Braga, S. d'Agostino, E. D'Amen, F. Grepioni, D. Genovese, L. Prodi and M. Sgarzi, *Dalton Trans.*, 2013, **42**, 16949–16960.

31 V. J. Anderson and H. N. W. Lekkerkerker, *Nature*, 2002, **416**, 811–815.

32 (*a*) O. Lebel, M.-E. Perron, T. Maris, S. F. Zalzal, A. Nanci and J. D. Wuest, *Chem. Mater.*, 2006, **18**, 3616–3626; (*b*) P. Terech, N. M. Sangeetha and U. Maitra, *J. Phys. Chem. B*, 2006, **110**, 15224–15233; (*c*) P. Zhu, X. Yan, Y. Su, Y. Yang and J. Li, *Chem.–Eur. J.*, 2010, **16**, 3176–3183; (*d*) D. J. Adams, K. Morris, L. Chen, L. C. Serpell, J. Bacsa and G. M. Day, *Soft Matter*, 2010, **6**, 4144–4156.

33 (*a*) C. D. Jones and J. W. Steed, *Chem. Soc. Rev.*, 2016, **45**, 6546–6596; (*b*) A. Dawn and H. Kumari, *Chem.–Eur. J.*, 2018, **24**, 762–776.

34 (*a*) R. S. Clegg and J. E. Hutchison, *Langmuir*, 1996, **12**, 5239–5243; (*b*) R. E. Richards and H. W. Thompson, *J. Chem. Soc.*, 1947, **237**, 1248–1260.

35 (*a*) G. Yu, X. Yan, C. Han and F. Huang, *Chem. Soc. Rev.*, 2013, **42**, 6697–6722; (*b*) J. Zhong, X. Jia, H. Liu, X. Luo, S. Hong, N. Zhang and J. Huang, *Soft Matter*, 2016, **12**, 191–199.

36 (*a*) N. Falcone and H. B. Kraatz, *Chem.–Eur. J.*, 2018, **24**, 1–14; (*b*) M. W. Tibbitt, J. E. Dahlman and R. Langer, *J. Am. Chem. Soc.*, 2016, **138**, 704–717; (*c*) K. J. Skilling, F. Citossi, T. D. Bradshaw, M. Ashford, B. Kellama and M. Marlow, *Soft Matter*, 2014, **10**, 237–256; (*d*) S. Cao, X. Fu, N. Wang, H. Wang and Y. Yang, *Int. J. Pharm.*, 2008, **357**, 95–99.

37 J. Dredán, I. Antal and I. Rácz, *Int. J. Pharm.*, 1996, **145**, 61–64.

38 (*a*) C. Fan, Y. Ling, W. Deng, J. Xue, P. Sun and D. Wang, *Biomed. Mater.*, 2019, **14**, 055006; (*b*) C. J. Fan and D. A. Wang, *Macromol. Biosci.*, 2015, **15**, 535–545.